Atomic-Scale Surface Segregation in Copper-Gold Nanoparticles

Grégoire Breyton,[1,2] Hakim Amara,[1,2] Jaysen Nelayah,[1] Jérôme Creuze,[3] Hazar Guesmi,[4] Damien Alloyeau,[1] Guillaume Wang,[1] and Christian Ricolleau[1,*]

[1]*Université Paris Cité, CNRS, Laboratoire Matériaux et Phénomènes Quantiques (MPQ), 75013 Paris, France*
[2]*Laboratoire d'Etude des Microstructures, ONERA-CNRS, UMR104, Université Paris-Saclay, BP 72, Châtillon Cedex, 92322, France*
[3]*ICMMO/ESP2M, Université Paris-Saclay, UMR 8182, 17 avenue des sciences, 91405 Orsay cedex, France*
[4]*ICGM ICMMM—Institut Charles Gerhardt Montpellier—Institut de Chimie Moléculaire et des Matériaux de Montpellier, Montpellier, France*

(Received 5 October 2022; revised 25 January 2023; accepted 12 May 2023; published 9 June 2023)

We combine electron microscopy measurements of the surface compositions in Cu-Au nanoparticles and atomistic simulations to investigate the effect of gold segregation. While this mechanism has been extensively investigated within Cu-Au in the bulk state, it was never studied at the atomic level in nanoparticles. By using energy dispersive x-ray analysis across the (100) and (111) facets of nanoparticles, we provide evidence of gold segregation in Cu_3Au and $CuAu_3$ nanoparticles in the 10 nm size range grown by epitaxy on a salt surface with high control of the nanoparticles morphology. To get atomic-scale insights into the segregation properties in Cu-Au nanoparticles on the whole composition range, we perform Monte Carlo calculations employing *N*-body interatomic potentials highlighting a complete segregation of Au in the (100) and (111) facets for gold nominal composition above 70% and 60%, respectively. Furthermore, we show that there is no size effect on the segregation behavior since we evidence the same oscillating concentration profile from the surface to the nanoparticle's core as in the bulk. These results shed new light on the interpretation of the enhanced reactivity, selectivity, and stability of Cu-Au nanoparticles in various catalytic reactions.

DOI: 10.1103/PhysRevLett.130.236201

Surface segregation in A_xB_{1-x} binary alloys, i.e., the enrichment of the surface by one of the elements as compared to the bulk composition, has been the subject of numerous studies [1–4]. It is a very important phenomenon in surface physics of alloys since it can dramatically change the intrinsic properties of the bulk material. Notably, it can strongly modify the surface reactivity of the alloys during catalytic reactions [5,6]. Three physical parameters are used to determine *a priori* the element that segregates at the surface [7]. The first two are the surface energy and the atomic size of the species that constitute the alloy. It is generally admitted that the element with the lower surface energy and with the larger size will segregate [8–10]. Another driving force is the alloying effect, meaning the competition between the cohesive energy of each individual atoms of the alloy and the free energy of mixing. These key quantities explaining segregation phenomena have been put forward by using phenomenological models based on pair-based [11–13] and elastic-strain energy theories [8,14]. Moreover, numerical calculations were performed within the tight-binding approximation to characterize the surface segregation from a microscopic point of view with an accurate description of the chemical bonds in transition metal based alloys [3,15–19].

In bulk CuAu alloys, this effect has been extensively studied from both experimental and theoretical approaches as a model system for binary alloys [9,10,20–30]. Among the most common ones, the techniques that were used to probe the surface composition of bulk Cu-Au are Auger electron spectroscopy (AES) [20–22], low energy ion scattering (LEIS) [9,23,24], low-energy electron diffraction (LEED) [24], and x-ray surface diffraction [25,26]. All of these works have shown various extents of Au surface segregation depending on the nature of the material (mono- vs polycrystal), the experimental technique, and the indexes of the considered surfaces. Interestingly, this segregation effect is followed by an oscillating concentration profile from the surface to the core of the material where the nominal concentration is finally reached [23,25,31,32].

For nanoparticles (NPs), the situation may change due to the so-called size effect, i.e., the competition between the bulk and surface energies of the NP [33] resulting in segregation effects as in the cases of Ag-Pt [34], Cu-Ag [35], or Ni-Pt [36] NPs. Indeed, physics at the nanoscale could be different than in bulk, especially for NPs smaller than around 10 nm. Typical examples include the dependence on the size of the melting temperature [37], surface energy [38] or mechanical properties [39] of pure NPs as well as the order-disorder transition temperature for bimetallic nanoalloys [40]. Regarding segregation effects in Cu_xAu_{1-x} NPs, very few studies exist. Results are mainly obtained by atomistic calculations [27–30,41]

and nanothermodynamic approaches [10]. All these works demonstrated Au segregation at the surface of the NPs. In one case, Cu enrichment of the NPs facets was also demonstrated, although this configuration is not stable [30]. From experiments, two papers report results on this system [10,30]. The segregation effect was evidenced by chemical mapping acquired by x-ray spectroscopy using transmission electron microscopy (TEM) in scanning mode (STEM). In these works, the Au segregation was revealed at the nanometer scale and in consequence there is no evidenceof the different extents of the segregation on the three main low index facets, namely, (111), (110), and (100), as observed in bulk systems. Indeed, such analysis along a NP, which is much more complex, has never been addressed.

In this Letter, we determine at the atomic scale the chemical composition of individual facets of epitaxially grown $CuAu_3$ and Cu_3Au NPs on a NaCl (100) surface in a truncated octahedral shape by using x-ray spectroscopy in an aberration-corrected electron microscope. We then compared the results to Monte Carlo simulations allowing the determination of the composition of (111) and (100) facets of Cu-Au NPs in the whole composition range. We show a remarkably good agreement between both approaches proving unambiguously the segregation of gold on NP surfaces at the atomic scale followed by an oscillating concentration profile within the particle.

From an experimental point of view, the challenge to evidence unambiguously the effect of Cu or Au segregation is to have perfect control on the 3D morphology of the NPs and then on the facets exhibited by the particles. For that purpose, we developed the epitaxial growth of CuAu NPs on a NaCl substrate and deposited them on a TEM carbon grid by the carbon replica technique [42]. The salt is dissolved in distilled water avoiding the possible elastic effects that can be generated in its presence. Cu-Au NPs were synthesized by the alternated pulsed laser deposition technique in a high vacuum chamber under a pressure of 10^{-8} Torr [43]. Two compositions were prepared in the Cu_3Au and $CuAu_3$ stoichiometry ranges and the growth was made at 400 ° C in order to obtain NPs in the fcc disordered phase ($A1$ phase). Experimental details are given in Sec. I of the Supplemental Material [44]. The NPs were imaged by using a double aberration corrected electron microscope (JEOL ARM 200F cold FEG) in STEM mode using the high angle annular dark field (HAADF) technique. Chemical analysis of the NP's surface composition was performed by energy dispersive x-ray spectroscopy (EDX).

Figure 1(a) shows a typical HAADF high resolution STEM image of a $CuAu_3$ stoichiometry NP oriented along the [011] zone axis. The exact composition measured by EDX spectroscopy over the whole NP is $Cu_{15}Au_{85}$. Through this projection, we clearly identify a truncated octahedron exhibiting six facets, namely, two (200) and four (111) ones, parallel to the electron beam. Since the fast Fourier transform (FFT) pattern of the NP does not show any superstructure reflections, the NP is in the $A1$ phase. We analyze the composition of (200) planes from the surface to the core of the NP across a line scan of the beam along the [200] direction to the planes [Fig. 1(a)]. The procedure is described in Sec. II of the Supplemental Material [44]. From each spectrum acquired along this line, we quantified the composition of an atomic column belonging to the (200) planes by analyzing the intensities under the Au-L_α and Cu-K_α edges using the Cliff-Lorimer method with a theoretical $k_{Cu/Au}$ [57] factor. The results are plotted as a function of the position of the beam along the line scan and shown in Fig. 1(b). Since the alloy is in the solid solution phase state, each site is randomly occupied by Cu or Au atoms with a probability of 0.15 and 0.85, respectively. Each column being equivalent in the lack of segregation, its composition is thus equal to the one of the atomic plane. From Fig. 1(b), it clearly appears that the (200) surface plane (atomic layer 1) is made of pure gold and then the composition tends to $Cu_{15}Au_{85}$ for the planes

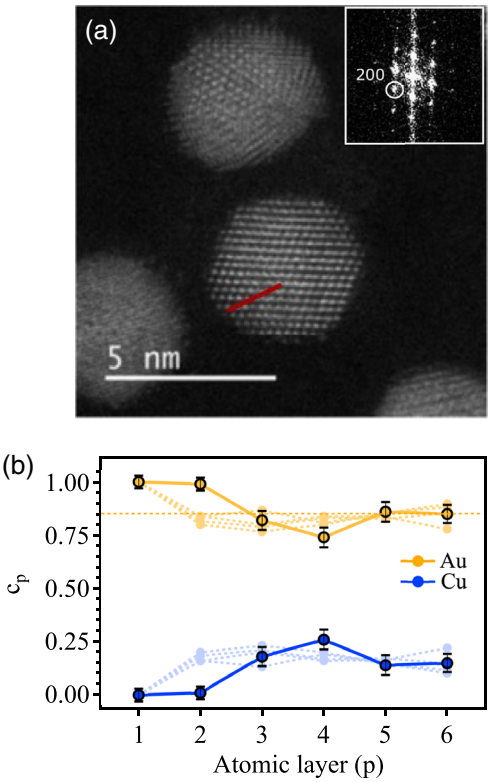

FIG. 1. (a) HRSTEM image of a $Cu_{15}Au_{85}$ NP oriented along the [011] zone axis. Inset: FFT of the image showing the [200] direction. Red line: direction of the line scan for the EDX analysis. (b) Composition profile in Au and Cu as a function of the position of the plane along the [200] direction from the surface (atomic layer 1) to the core of the NP. Light colors: Au and Cu concentrations extracted from the atomistic simulations performed on a NP with the same nominal composition along the same family of planes as the experimental ones.

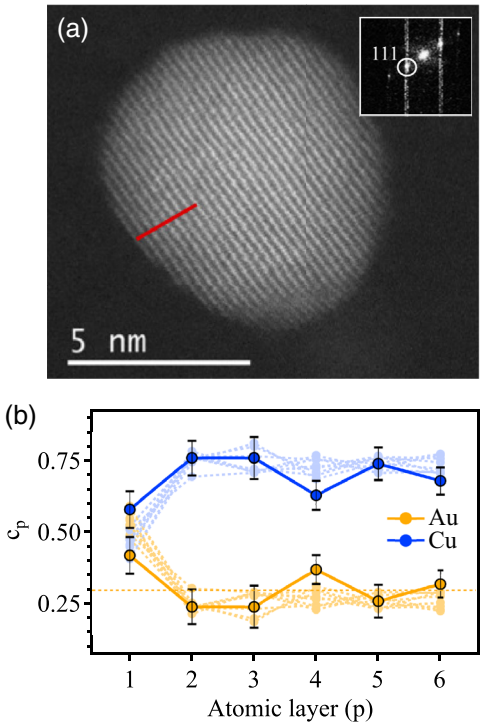

FIG. 2. (a) HRSTEM image of a $Cu_{70}Au_{30}$ NP oriented near the [110] zone axis. Inset: FFT of the image showing the [111] direction. Red line: directions of the line scan for the EDX analysis. (b) Composition profile in Au and Cu as a function of the position of the plane along the [111] direction from the surface (atomic layer 1) to the core of the NP. Light colors: Au and Cu concentrations extracted from the atomistic simulations performed on a NP with the same nominal composition along the same family of plane as the experimental ones.

belonging to the core of the NP. It should be pointed out that in this composition range, i.e., in the Au rich region of the phase diagram of the Cu-Au system, when the first surface plane is saturated in gold, the subsequent planes become enriched with copper to reach the nominal composition of the alloy [Fig. 1(b)]. Note that in addition to the accuracy of the EDX technique without a reference sample which is around 5 at.%, the precision of the analysis is very sensitive to the exact alignment of the plane with respect to the electron beam: a small misalignment may cause the spectrum to not strictly correspond to the composition of a unique atomic column.

For the Cu_3Au stoichiometry, a HAADF image of a $Cu_{70}Au_{30}$ NP is shown in Fig. 2(a). The nanoparticle is oriented near the [110] zone axis and the corresponding FFT pattern exhibits the 111 reflections. No superstructure reflexions are observed confirming that the NP is in the disordered FCC state. Hence, the expected composition of these planes must be $Cu_{70}Au_{30}$. We analyzed the plane compositions from the surface to the core along a line scan perpendicular to the (111) surface following the same procedure as before. The results are plotted in Fig. 2(b). According to these concentration profiles, it appears clearly that the composition of the (111) surface is enriched in gold meaning 42% instead of 30% according to the NP's composition and a depletion in copper, 58% instead of 70%. The nominal composition of the plane is recovered from the second plane.

To get insight into the segregation properties of Cu-Au NPs at atomic scale, we perform simulations using an N-body potential derived from the second moment approximation (SMA) of the tight-binding (TB) scheme [58,59] implemented into a Monte Carlo (MC) code to relax the structures [60]. Here, the simulations are performed at high temperatures to ensure that the NPs are in a disordered state as it is the case experimentally. Regarding the TB-SMA potential and the MC calculations, more details can be found in Sec. III of the Supplemental Material [44]. Meanwhile, we note that the calculated Au surface energies are lower than those of Cu, in line with *ab initio* calculations, favoring Au surface segregation. Since we focus on segregation phenomena, we have ensured that our TB potential can satisfactorily reproduce the enthalpy of segregation of the solute at the surface, ΔH^{seg}. Indeed, the tendency of a constituent to segregate is characterized by this quantity defined as the energy balance involved when one atom of a given species, initially placed in the bulk, is exchanged with an atom of the other species located at the surface [61,62]. A negative value of ΔH^{seg} means that solute segregation is favored. As shown in Sec. III of the Supplemental Material [44], our TB-SMA results are in agreement with the *ab initio* data. More precisely, we notice a strong tendency for the Au impurity to segregate on the first layer and this whatever the Cu surface considered, namely, (100), (111), and (101). The conclusions are rather different in the case of the copper solute where opposite behavior is observed. Even if the alloying effect should obviously not be neglected, we can expect to observe a strong segregation of Au within NPs through our simulations and quantify more accurately this phenomenon at the atomic scale.

We considered truncated octahedron Cu-Au NPs containing 405, 1289, and 4033 atoms. This corresponds to cluster sizes around 2 to 5 nm close to the range explored experimentally. Figure 3(a) depicts the segregation isotherms for a Cu-Au NP in a disordered state containing 4033 atoms with initial composition covering the whole phase diagram. Obviously, our simulations show that Au segregates whatever its nominal concentration, with complete segregation when the gold concentration exceeds 70%. Concomitantly, we observe a depletion in Au atoms in the first two sublayers. Beyond that, a progressive return to the nominal concentration is achieved. To go further, surface concentrations of different facets are analyzed in Fig. 3(b). Interestingly, there is an enhancement of Au enrichment when going from the close-packed (111) facet to the open (100) one, in agreement with usual surface energy arguments [61]. Gold enrichment is therefore

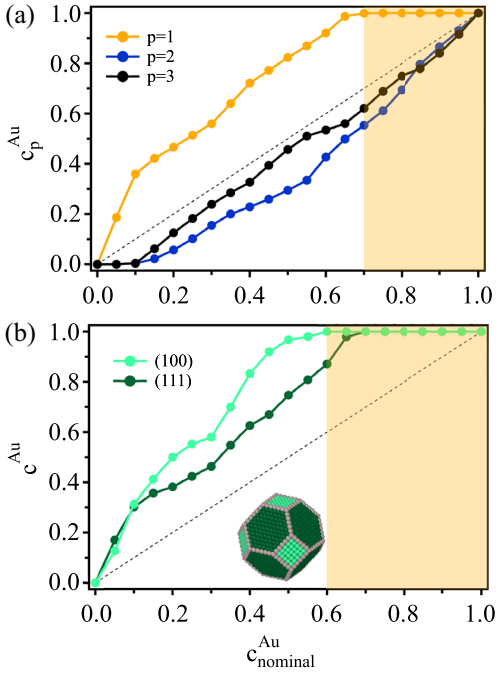

FIG. 3. Segregation isotherms in the disordered state for (a) the surface ($p = 1$) and the first two sublayers ($p = 2, 3$) and (b) the (100) and (111) surfaces for the truncated octahedron Cu-Au nanoalloys containing 4033 atoms.

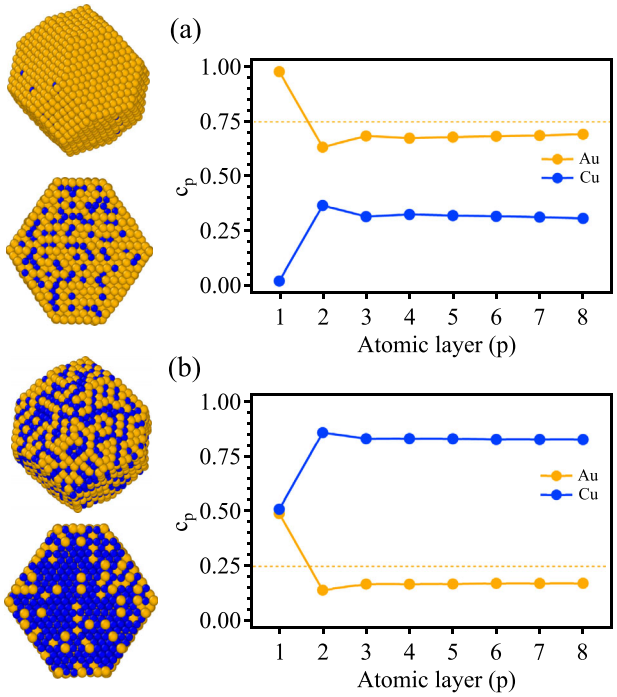

FIG. 4. Cross-section views of a characteristic equilibrium configuration and concentration profiles along the radius of a NP containing 4033 atoms after performing MC simulations in the disordered state. (a) $CuAu_3$ and (b) Cu_3Au.

strongly favored on a (100) surface compared to a (111) one, resulting in a complete saturation from a nominal concentration of 60 at.% gold.

We now focus on specific concentrations where ordered phases exist, i.e., $CuAu_3$ and Cu_3Au [63]. Let us start with the $CuAu_3$ composition in a disordered state. After performing MC simulations, strong segregation effects are highlighted. A visual inspection depicts a NP completely surrounded by a thin layer of gold as seen in Fig. 4(a). The innermost layers do not show any particular gold enrichment but display a random structure typical of a disordered state. This is confirmed in a more quantitative way with the analysis of the density profiles along the radius of the NPs. The first layer is completely enriched in gold then the concentration decreases within the NP to get closer to the nominal concentration of 75% of Au. In a second step, Cu_3Au NPs are addressed and exhibit a much less striking segregation effect. As seen in Fig. 4(b), only 50% of the surface is covered with Au. Although a significant enrichment of the surface in gold is observed (about twice the nominal concentration), our simulations do not show a complete Au layer surrounding the NP. Consequently, atomistic simulations confirm that Au segregates at the surface of NPs whatever their composition and size.

To compare quantitatively the experimental measurements to the numerical calculations, we extracted from the atomistic simulations the concentration profiles of each plane from the surface as acquired in the TEM. For that purpose, we determine for the $Cu_{15}Au_{85}$ composition, the concentration of each column of the (200) planes. The composition profiles for each atomic column, for different line scans, are superimposed on the experimental curves in Fig. 1(b). The same procedure was applied for the $Cu_{70}Au_{30}$ composition [see Fig. 2(b)]. For both compositions, we show a remarkably good quantitative agreement between both results. In particular, due to the intrinsic statistical nature of the FCC disordered phase, the experimental curves are situated in between the two envelope curves determined from the numerical model. Moreover, we prove without any ambiguity the effect of Au segregation on these planes for these alloy stoichiometries.

Knowing the real composition of the surface of bimetallic NPs is crucial for their applications. Regarding Cu_xAu_{1-x} NPs, we succeeded in showing the segregation of a single layer of Au at the surface thus addressing an existing debate in the literature. This has been achieved by combining measurements of the surface composition of (100) and (111) surfaces of NPs with controlled morphology and atomic-scale simulations. Moreover, our analysis has proven a concentration profile from the facets to the core of the NP as already discussed in infinite surfaces highlighting that such a mechanism is still present at the nanoscale. No specific features are found for the two disordered NPs studied here. Differences can be observed if concentration profiles across ordered NPs are investigated where segregation profiles differ according to the composition with a high dependence on the facet indexes

considered. This is currently under progress. The conclusions presented here are essential for the surface and catalyst community [36] since they highlight how it is crucial to consider the real surface composition and the concentration profile along the NPs to analyze their reactivities. This work constitutes a major step, showing that the future to understand catalysis of nanoalloys is to determine the complete concentration profile of the NP surfaces under real environmental conditions since segregation behavior can be changed [64].

The authors thank ANR GIANT (No. ANR-18-CE09-0014-04). H. A. thanks B. Legrand for fruitful discussions. The authors acknowledge the Region Ile-de-France for convention SESAME E1845 for the support of the JEOL ARM 200 F electron microscope installed at the Paris Cité University.

*christian.ricolleau@u-paris.fr

[1] M. A. Vasiliev, Surface effects of ordering in binary alloys, J. Phys. D **30**, 3037 (1997).
[2] J. R. Chelikowsky, Predictions for surface segregation in intermetallic alloys, Surf. Sci. **139**, L197 (1984).
[3] C. A. Balseiro and J. L. Morán-López, Electronic theory for surface segregation: Noble-metal alloys, Phys. Rev. B **21**, 349 (1980).
[4] V. Poneç, *Electronic Structure and Reactivity of Metal Surfaces* (Plenum, New York, 1976).
[5] M. Okada, Y. Tsuda, K. Oka, K. Kojima, Wilson A. Diño, A. Yoshigoe, and H. Kasai, Experimental and theoretical studies on oxidation of Cu-Au alloy surfaces: Effect of bulk Au concentration, Sci. Rep. **6**, 31101 (2016).
[6] S. Nakanishi, K. Kawamoto, N. Fukuoka, and K. Umezawa, Low energy ion scattering analysis of the surface compositional change of Au_3Cu (001) induced by oxygen chemisorption, Surf. Sci. **261**, 342 (1992).
[7] P. Wynblatt and R. C. Ku, Surface energy and solute strain energy effects in surface segregation, Surf. Sci. **65**, 511 (1977).
[8] D. McLean, *Grain Boundaries in Metals* (Oxford University, London, 1957).
[9] M. J. Sparnaay and G. E. Thomas, Surface segregation in $Au_{0.1}Cu_{0.9}$ crystals, Surf. Sci. **135**, 184 (1983).
[10] G. Guisbiers, S. Mejia-Rosales, S. Khanal, F. Ruiz-Zepeda, R. L. Whetten, and M. José-Yacaman, Gold-copper nanoalloy, tumbaga, in the era of nano: Phase diagram and segregation, Nano Lett. **14**, 6718 (2014).
[11] F. L. Williams and D. Nason, Binary alloy surface compositions from bulk alloy thermodynamic data, Surf. Sci. **45**, 377 (1974).
[12] R. A. Van Santen and W. M. H. Sachtler, A theory of surface enrichment in ordered alloys, J. Catal. **33**, 202 (1974).
[13] J. L. Morán-López and K. H. Bennemann, Surface effects on the order-disorder phase transition of A_3B alloys, Phys. Rev. B **15**, 4769 (1977).
[14] J. J Burton and R. S Polizzotti, Surface segregation in alloys: Dilute solid solutions of Cr, Fe and Ni in Pt, Surf. Sci. **66**, 1 (1977).
[15] C. Mottet, G. Tréglia, and B. Legrand, Theoretical investigation of chemical and morphological ordering in Pd_cCu_{1-c} clusters, Phys. Rev. B **66**, 045413 (2002).
[16] B. Legrand, G. Tréglia, and F. Ducastelle, Phase transitions in surface segregation of Pt_cNi_{1-c} alloys from Tight-Binding Ising-Model calculations, Phys. Rev. B **41**, 4422 (1990).
[17] G. Tréglia and B. Legrand, Surface-sandwich segregation in Pt-Ni and Ag-Ni alloys: Two different physical origins for the same phenomenon, Phys. Rev. B **35**, 4338 (1987).
[18] G. Kerker, J. L. Morán-López, and K. H. Bennemann, Electronic theory for segregation at the surface of transition-metal alloys, Phys. Rev. B **15**, 638 (1977).
[19] Ph. Lambin and J. P. Gaspard, Electronic theory of surface segregation in CuNi alloys, Solid State Commun. **28**, 123 (1978).
[20] S. Mróz, Composition of the first atomic layers of (001)-oriented $AuCu_3$ crystal measured with the use of directional auger electron spectroscopy at $400\ \mathrm{K} < \mathrm{T} < 1000\ \mathrm{K}$, Vacuum **79**, 241 (2005).
[21] S. Mróz and A. Krupski, Composition of the first two atomic layers in $Au_{0.2}Cu_{0.8}$ and $Au_{0.8}Cu_{0.2}$ alloys, Vacuum **60**, 307 (2001).
[22] J. M. McDavid and S. C. Fain, Segregation at Cu-Au alloy surfaces, Surf. Sci. **52**, 161 (1975).
[23] T. M. Buck, G. H. Wheatley, and L. Marchut, Order-Disorder and Segregation Behavior at the $Cu_3Au(001)$ Surface, Phys. Rev. Lett. **51**, 43 (1983).
[24] E. G. McRae, T. M. Buck, R. A. Malic, W. E. Wallace, and J. M. Sanchez, Ordering and layer composition at the $Cu_3Au(110)$ surface, Surf. Sci. **238**, L481 (1990).
[25] H. Reichert, P. J. Eng, H. Dosch, and I. K. Robinson, Thermodynamics of Surface Segregation Profiles at $Cu_3Au(001)$ Resolved by X-Ray Scattering, Phys. Rev. Lett. **74**, 2006 (1995).
[26] H. Reichert and H. Dosch, Surface segregation in $Cu_3Au(001)$, Surf. Sci. **345**, 27 (1996).
[27] D. Cheng, S. Huang, and W. Wang, The structure of 55-atom Cu-Au bimetallic clusters: Monte Carlo study, Eur. Phys. J. D **39**, 41 (2006).
[28] N. T. Wilson and R. L. Johnston, A theoretical study of atom ordering in copper-gold nanoalloy clusters, J. Mater. Chem. **12**, 2913 (2002).
[29] B. Pauwels, G. Van Tendeloo, E. Zhurkin, M. Hou, G. Verschoren, L. T. Kuhn, W. Bouwen, and P. Lievens, Transmission electron microscopy and Monte Carlo simulations of ordering in Au-Cu clusters produced in a laser vaporization source, Phys. Rev. B **63**, 165406 (2001).
[30] J. A. Ascencio, H. B. Liu, U. Pal, A. Medina, and Z. L. Wang, Transmission electron microscopy and theoretical analysis of AuCu nanoparticles: Atomic distribution and dynamic behavior, Microsc. Res. Technol. **69**, 522 (2006).
[31] M. Hayoun, V. Pontikis, and C. Winter, Computer simulation study of surface segregation on Cu_3Au, Surf. Sci. **398**, 125 (1998).
[32] M. Hou and M. El Azzaoui, A Monte Carlo study of the thermal properties of Cu_3Au low index surfaces, Surf. Sci. **380**, 210 (1997).

[33] L. Peng, E. Ringe, R. P. Van Duyne, and L. D. Marks, Segregation in bimetallic nanoparticles, Phys. Chem. Chem. Phys. **17**, 27940 (2015).
[34] J. Pirart, A. Front, D. Rapetti, C. Andreazza-Vignolle, P. Andreazza, C. Mottet, and R. Ferrando, Reversed size-dependent stabilization of ordered nanophases, Nat. Commun. **10**, 1982 (2019).
[35] C. Langlois, Z. L. Li, J. Yuan, D. Alloyeau, J. Nelayah, D. Bochicchio, R. Ferrando, and C. Ricolleau, Transition from core-shell to Janus chemical configuration for bimetallic nanoparticles, Nanoscale **4**, 3381 (2012).
[36] C. Cui, L. Gan, M. Heggen, S. Rudi, and P. Strasser, Compositional segregation in shaped Pt alloy nanoparticles and their structural behaviour during electrocatalysis, Nat. Mater. **12**, 765 (2013).
[37] Ph. Buffat and J-P. Borel, Size effect on the melting temperature of gold particles, Phys. Rev. A **13**, 2287 (1976).
[38] H. Amara, J. Nelayah, J. Creuze, A. Chmielewski, D. Alloyeau, C. Ricolleau, and B. Legrand, Effect of size on the surface energy of noble metal nanoparticles from analytical and numerical approaches, Phys. Rev. B **105**, 165403 (2022).
[39] J. Amodeo and L. Pizzagalli, Modeling the mechanical properties of nanoparticles: A review, C.R. Phys. **22**, 35 (2021).
[40] D. Alloyeau, C. Ricolleau, C. Mottet, T. Oikawa, C. Langlois, Y. Le Bouar, N. Braidy, and A. Loiseau, Size and shape effects on the order-disorder phase transition in CoPt nanoparticles, Nat. Mater. **8**, 940 (2009).
[41] J. Li, G. Wang, and G. Zhou, Surfaces segregation phenomena in extended and nanoparticle surfaces of Cu-Au alloys, Surf. Sci. **649**, 39 (2016).
[42] V. Pierron-Bohnes, I. Florea, O. Ersen, C. Ulhaq-Bouillet, C. Goyhenex, N. Braidy, C. Ricolleau, Y. Le Bouar, and D. Alloyeau, Atomic-scale faceting in CoPt nanoparticles epitaxially grown on NaCl, Cryst. Growth Des. **14**, 2201 (2014).
[43] D. Alloyeau, C. Langlois, C. Ricolleau, Y. Le Bouar, and A. Loiseau, A TEM in situ experiment as a guideline for the synthesis of as-grown ordered CoPt nanoparticles, Nanotechnology **18**, 375301 (2007).
[44] See Supplemental Material at http://link.aps.org/supplemental/10.1103/PhysRevLett.130.236201 for additional TEM data, technical explanation to clarify experimental (EDX) measurements and sample preparation, as well as details on the second moment approximation interatomic potential, Monte Carlo simulations and DFT calculations which includes Refs. [45–56].
[45] C. Kittel, *Introduction to Solid State Physics*, 7th ed. (Wiley, New York, 1995).
[46] G. Simmons and H. Wang, *Single Crystal Elastic Constants and Calculated Aggregates Properties* (MIT, Cambridge, 1971).
[47] L. Vitos, A. V. Ruban, H. L. Skriver, and J. Kollár, The surface energy of metals, Surf. Sci. **411**, 186 (1998).
[48] M. S. S. Brooks and B. Johansson, Exchange integral matrices and cohesive energies of transition metal atoms, J. Phys. F **13**, L197 (1983).
[49] J. Guevara, A. M. Llois, and M. Weissmann, Model potential based on tight-binding total-energy calculations for transition-metal systems, Phys. Rev. B **52**, 11509 (1995).
[50] C. Barreteau, F. Raouafi, M. C. Desjonquères, and D. Spanjaard, The phonon spectra and vibrational thermodynamical properties of Cu vicinal surfaces, Surf. Sci. **519**, 15 (2002).
[51] C. Goyhenex, Revised tight-binding second moment potential for transition metal surfaces, Surf. Sci. **606**, 325 (2012).
[52] R. Hultgren, P. D. Desai, D. T. Hawkins, M. Geiser, and K. K. Kelly, *Selected Values of the Thermodynamic Properties of Binary Alloys* (Wiley, New York, 1973).
[53] P. E. Blöchl, O. Jepsen, and O. K. Andersen, Improved tetrahedron method for brillouin-zone integrations, Phys. Rev. B **49**, 16223 (1994).
[54] G. Kresse and D. Joubert, From ultrasoft pseudopotentials to the projector augmented-wave method, Phys. Rev. B **59**, 1758 (1999).
[55] G. Kresse and J. Hafner, Ab initio molecular dynamics for liquid metals, Phys. Rev. B **47**, 558 (1993).
[56] J. P. Perdew and Y. Wang, Accurate and simple analytic representation of the electron-gas correlation energy, Phys. Rev. B **45**, 13244 (1992).
[57] G. Cliff and G. W. Lorimer, The quantitative analysis of thin specimens, J. Microsc. **103**, 203 (1975).
[58] F. Ducastelle, Module élastique des métaux de transition, J. Phys. (Paris) **31**, 1055 (1970).
[59] V. Rosato, M. Guillopé, and B. Legrand, Thermodynamical and structural properties of f.c.c. transition metals using a simple tight-binding model, Philos. Mag. A **59**, 321 (1989).
[60] D. Frenkel and B. Smith, *Understanding Molecular Simulations* (Academic Press, London, 2002).
[61] G. Tréglia, B. Legrand, F. Ducastelle, A. Saúl, C. Gallis, I. Meunier, C. Mottet, and A. Senhaji, Alloy surfaces: Segregation, reconstruction and phase transitions, Comput. Mater. Sci. **15**, 196 (1999).
[62] J. Creuze, H. Guesmi, C. Mottet, B. Zhu, and B. Legrand, Surface segregation in AuPd alloys: Ab initio analysis of the driving forces, Surf. Sci. **639**, 48 (2015).
[63] H. Okamoto, D. J. Chakrabarti, D. E. Laughlin, and T. B. Massalski, The Au-Cu (Gold-Copper) system, Bull. Alloy Phase Diagrams **8**, 454 (1987).
[64] B. Zhu, G. Thrimurthulu, L. Delannoy, C. Louis, C. Mottet, J. Creuze, B. Legrand, and H. Guesmi, Evidence of Pd segregation and stabilization at edges of AuPd nano-clusters in the presence of CO: A combined DFT and drifts study, J. Catal. **308**, 272 (2013).